We are IntechOpen, the world's leading publisher of Open Access books Built by scientists, for scientists

6,900
Open access books available

185,000
International authors and editors

200M
Downloads

Our authors are among the

154
Countries delivered to

TOP 1%
most cited scientists

12.2%
Contributors from top 500 universities



WEB OF SCIENCE™

Selection of our books indexed in the Book Citation Index in Web of Science™ Core Collection (BKCI)

Interested in publishing with us?
Contact book.department@intechopen.com

Numbers displayed above are based on latest data collected.
For more information visit www.intechopen.com



Chapter

Wave Drag Modification in the Presence of Discharges

Anna Markhotok

Abstract

A phenomenological model of wave drag modification following the thermal energy deposition in a hypersonic flow is presented. While most of the previous research was concentrated on finding optimal gas parameter values and the amount of energy, this work points at closer attention to the effect of the parameter distribution and the geometry of experimental arrangements. The approach discussed here is to fill the gap in the understanding of the complex mechanism of the flow transformation leading to the wave drag reduction. Analytical expressions used in the model identify a number of adjustment parameters that can be used to optimize thermal energy input and thus achieve fundamentally lower drag values than that of conventional approaches.

Keywords: shock waves, hypersonic plasma dynamics, shock wave instability, vorticity, aerodynamics drag

1. Introduction

The drag is one of the four major forces acting on an airplane in flight. Depending on the nature of the body-flow interaction and the phase of flight, it can be divided into three basic components. The pressure drag is due to pressure distribution over the vehicle surface and skin friction. The induced drag results from the pressure redistribution following the formation of the trailing vortex system during the lift production and thus becomes significant only during takeoff and landing times. When the free stream Mach number exceeds 0.8, the local flow velocities at some points on the airframe may become supersonic, and shock waves set in at the corresponding locations. The gas compression in a shock wave results in the pressure increase in the flow in front of the moving body. This is usually felt as an abrupt increase in local drag and reduction in local lift that may be accompanied by associated changes in trim, pitching moment, and the stability and control characteristics of the airplane. This portion of the drag, the so-called wave drag, is up to four times larger than its subsonic component and can result in the aerodynamic efficiency reduced by more than 50%. The wave drag is the reason for the strong pushback (shock stall) an aircraft experiences when, during acceleration through the transonic flight regime, the Mach number first reaches its critical value and the local speed passes through the sonic point ("sonic barrier"). The increase in the drag by 1% is equivalent to 5–10% of payload, and thus it imposes significant limitations on the speed, range, and payload carried by a vehicle [1].

The shock wave weakening achieved by altering the shock formation processes is one of the efficient methods developed to reduce the wave drag. Swept wing

IntechOpen

surface minimizes the shock strength, thereby reducing wave drag. Sweeping beyond the Mach line converts the wing design problem into a transonic issue and also enables extension into supersonic speeds of "leading edge thrust" [1, 2]. Moving lift forward onto the fuselage allows extending the lifting line and reducing the drag due to lift [3]. This approach finally led to the so-called Coke bottle of the transonic fighter regime [4]. A method using an active or passive flow separation control at cruise has been suggested in [5].

The shock wave interaction with other components of the aircraft (centerbody-nacelle, nacelle-wing, body-wing, body-body, and body/wing-propulsion exhaust efflux) [1, 4] can be used to obtain favorable wave interference leading to a weakened shock system. Up to 25% reduction of the wave drag and increase in the lift-to-drag ratio were reported [6].

One of the approaches in which the shock energy is effectively redirected into the thrust production uses the interaction between the forebody shock with a wing raised above the body. The shock reflection onto the afterbody results in pressure increase and an increment of thrust. Though these methods were proven to be effective in a number of localized problems such as centerbody inlets and nacelle-wing interactions, significant difficulties were encountered in other applications [1].

The local passive porosity method [7] utilizes high transonic flow sensitivity to local geometry changes resulting in the replacement of strong shocks with a system of weaker ones (λ-shock system). Localized wall deformations/bumps were shown to weaken the shock wave through the generation of nearly isentropic waves upstream [8]. The trailing edge methods use truncation of the region or morphing trailing edge to alter the airfoil shape [9].

The "physical spikes" representing an artificial sharpening of the front region of a blunt body can reduce the drag up to 30–45% [10]. It works through the replacement of nearly normal shock wave with a weaker, oblique shock structure. The upstream inert gas jets or liquid/solid particles injected in front of the body [11] is another method of the same type; however, its effect is weakened by injection thrust in the drag direction.

Thermal energy deposited in the flow upstream of the body is another spike-like working approach reporting 20–30% drag reduction rates in experiments [5, 12, 13] and 40–96% (with 65-fold "return" of the invested energy) predicted in numerical studies [14]. The energy is delivered into the flow via RF, microwave, or optical discharge, with focused electron beam or localized combustion combined with the spike. Pulsed energy deposition methods have been shown to be more efficient than continuous if an appropriate repetition rate is chosen [15]. A combination of methods, such as simultaneous addition of the heat at the tip of the physical spike, leads to flow reattachment on the nose and can further reduce the drag up to 75% [1, 5]. The study showed that, under a number of simplifying assumptions, a thermally created phantom body enveloping the airplane results in finite rise-time signatures that can theoretically eliminate the shock wave, but practically this would require a power input approximately equivalent to twice that necessary to sustain the airplane flight. Thus, the idea of the thermal energy deposition in the flow can be practically realized if highly effective ways of the energy deposition and the shock-thermal area interaction are found.

Using different approaches in the heat design, some authors found little or no effect in the drag reduction. It is the main conclusion of many researchers that, for further progress, a careful design of the energy deposition must be applied. While most of the previous research was concentrated on finding optimal gas parameter values and the amount of energy, this work will point at the exact mechanism of the shock-plasma interaction. Recommendations in the form of adjustment parameters will be done based on closer attention to the effect of the gas parameter distribution

and the geometry of the interaction zone. A model providing an insight on the origin of the chain of consecutive transformations in the flow leading to the wave drag reduction can be used to optimize thermal energy input and thus achieve fundamentally lower drag values than that of conventional approaches.

In the interaction between a shock wave and a plasma region produced in a discharge, the initially simply structured planar, bow, or oblique shock wave loses its stability and eventually evolves into a complicated system of distorted and secondary shocks with flow separation regions and formation of vortices in the flow behind the shock [16, 17]. The main changes in the "shock-plasma" system include the shock's acceleration and its front distortion gradually increasing with time, followed with its weakening until it becomes unidentifiable [18, 19]; motion of the shock away from the body in the presence of heating [20]; substantial gas/plasma parameter redistribution in the flow behind the shock, particularly considerable reduction of gas pressure; a vortex system forming in the aftershock flow [12]; remarkable positive dynamics in the vortex strength as the shock propagates well beyond the interface suggesting not only boundary but volume effects as well; the time delays in the effects on the flow relative to the discharge on-off times and a finite pressure rise time [21]; and finally a strong distortion or collapse of the plasma region [22]. Similar phenomena are commonly observed in other settings involving the shock interacting with an interface: in the front separation region control experiments [23], in combustion [22], and in impulsively loaded flows having place in astrophysics plasmas [24] and fusion research [25]. The shock-flame interaction, where the instability induced by the shock wave passage through a flame results in a sharp increase of the burning velocity [26, 27], is used in the supersonic combustion for increased chemical reaction rates.

The existing models used to describe the observed phenomena can be split into two major approaches. The first one considering thermal heating as a possible reason includes Mach number decrease due to gas heating and the possibility of mean molecular weight and number density change caused by molecule dissociation and ionization [14]. The contribution of possible nonthermal mechanisms of the interaction is considered for flows involving atomic and molecular transitions, gas kinetics, electrical properties of plasmas, and non-equilibrium states as a result of fast evolving processes such as radiation or fast expansion. Among them are appearance of charged particles leading to upstream momentum transfer in the hypersonic flow [12, 28, 29]; the possibility of deflection of the incoming flow by plasma in front of the shock via electronic momentum transfer collisions [30]; and the release of heat into the shock layer by the exothermic reactions enhancing the shock layer temperature and thus reducing the pressure and the density behind the shock wave [31].

The baroclinic effect is one of the mechanisms that can be responsible for vorticity generation on an interface when there is nonalignment of pressure and density gradients in the hot gas region [32]. Richtmyer-Meshkov instability (RMI) takes place when two gases of different densities are accelerated by a passage of a shock wave. The acceleration causes growth of small perturbations of the interface, followed by a nonlinear regime with bubbles appearing in the case of lighter gas penetrating a heavier gas and with spikes appearing in the case of a heavier gas moving into the lighter one. The vortex sheet rolls up and accumulates into periodic vortex cores in the post-shock flow [21].

The previous research on this topic was quite successful in explaining some separate features of the interaction. However, the experiments show that each of the processes is not an isolated phenomenon and their coexistence and specific time sequence in their development cannot be covered by the existing models. The model described below is capable of explaining the full set of the features observed

in experiments and thus fills the gap in understanding of this phenomenon. The shock refraction on an interface will be considered there as a mechanism [33] that triggers the chain of subsequent flow transformations leading to the wave drag reduction. The model has an advantage of pointing at the origin of the complex phenomena and describing each of the consecutive stages of its development in adequate timing order.

2. Model of the interaction

It will be assumed here that a thermal spot (plasma region) has been created via a discharge at a distance in front of a stationary solid body and the spot's continuous expanding ceases by the time of interaction. This could be a case of a relatively slow evolving plasma bubble or when thermal energy is deposited far enough from the body, so the system had enough time to achieve a thermal equilibrium state. The plasma region is allowed to move with the hypersonic flow toward the bow shock formed in front of the body. The interaction starts when the plasma region arrives at the shock location, and that is when the time t in the model relations starts to be counted. For blunt bodies that are common in the experiments, a spherical shock wave and interface geometry can be an adequate approximation.

In **Figure 1**, the spherical interface (dashed curve) separates the hot plasma (medium 2) and the surrounding cold gas (medium 1). Both media will be treated as ideal gases with initially equal pressures on both sides of the interface.

The cold gas temperature T_1 will be always distributed homogeneously, and T_2 is the plasma temperature right behind the interface with varied parameter distribution along the shock motion direction. The gas temperature can change across the interface abruptly (stepwise) or smoothly (distributed over a distance) [34], and $T_2 > T_1$. The radii R_b and R_s are for the plasma boundary and the shock front correspondingly, and other parameters are shown in the figure. In the reference frame stationary for the plasma region, the shock wave is incident on the interface from left to right, center to center, with constant horizontal velocity V_1. If the hotter medium (plasma) is uniform, a portion of the shock front crossing the interface accelerates to velocity V_2 in a steplike manner, and after this its velocity remains constant. Due to the acceleration, this portion advances faster compared to the

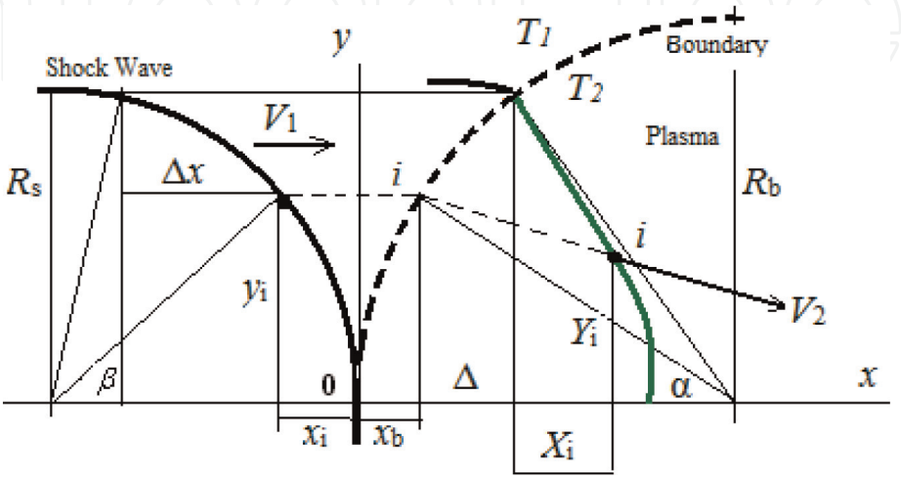


Figure 1.
Shock-plasma interaction diagram in the vertical plane of symmetry. As the initially spherical shock progresses through the spherical interface (dashed curve), its shape gradually deforms (green curve). Only the upper part of the diagram is shown.

reminder that is still propagating in the colder media thus resulting in the continuously increasing front stretching toward the hotter medium [18].

The shock front development proceeds in two stages, first being affected by the conditions on the interface and second in the plasma volume. The shock refraction resulting in an increase of the absolute value of the shock velocity along with its vector rotation (at refraction angle γ) occurs at the moment when the shock front crosses the plasma interface. As the refracted shock continues to propagate in hotter medium, its dynamics is determined by the parameter distribution in the plasma volume [17, 19, 33, 35]. Even though the changes in the shock structure become visible only during this time, they are the still consequences of the interaction at both stages: the conditions on the interface are necessary to trigger the front instability, and the gas volume effects provide the means necessary for its positive dynamics.

The relationship between the incident (x_i, y_i) and refracted (X_i, Y_i) shock front coordinates at a point of the interaction i has been derived in [33]. To recast it in a dimensionless form, the coordinates can be scaled with the plasma sphere radius R_b, the shock velocity with V_1, gas temperature with T_1, Mach number with M_{1n}, and time t with the characteristic time $\tau = R_b/V_1$:

$$\overline{X_i} = (\overline{v}\cos\gamma - 1)(n - (\overline{x_i} + \overline{x_b})) + \Delta\overline{x},\ \overline{Y_i} = \overline{y_i} - \overline{v}\sin\gamma \bullet (n - (\overline{x_i} + \overline{x_b})) \tag{1}$$

Here $n = t/\tau$ is the dimensionless time, $0 < n < 2$, α is the local incidence angle at the interaction point (**Figure 1**), $\overline{x_b} = 1 - \cos\alpha$, $\overline{\Delta x} = (R_s/R_b)(\cos\beta - \eta)$, the parameter

$$\eta = \frac{2(R_s + R_b)(R_s - nR_b) + n^2R_b^2}{2R_s[(R_s + R_b) - nR_b]} \tag{2}$$

and the bar over the variable means its dimensionless equivalent. The dimensionless shock velocity

$$\overline{v} = V_2/V_1 = \sqrt{\overline{T}\left(\overline{M}\right)^2\cos^2\alpha + \sin^2\alpha} \tag{3}$$

and the refraction angle $\gamma = \alpha - \tan^{-1}\left(\sqrt{\overline{TM}}\tan\alpha\right)$ are determined by the problem geometry, heating intensity $\overline{T} = T_2/T_1$, and the ratio of normal components of Mach numbers in the two media $\overline{M} = M_{2n}/M_{1n}$ that account for the shock reflections off the interface.

The Mach number ratio for normal incidence can be obtained using the refraction equation from [36] that was derived assuming steplike temperature T_2/T_1 changes across the interface (a "sharp" interface)

$$\frac{1}{M_{1n}(k-1)}\left\{\left[2kM_{1n}^2 - (k-1)\right]\left[(k-1)M_{1n}^2 + 2\right]\right\}^{\frac{1}{2}} \times \left\{\left[\frac{2kM_{2n}^2 - (k-1)}{2kM_{1n}^2 - (k-1)}\right]^{\frac{k-1}{2k}} - 1\right\}$$
$$= M_{1n}\left(1 - \frac{1}{M_{1n}^2}\right) - M_{2n}\left(1 - \frac{1}{M_{2n}^2}\right)\left(\frac{T_2}{T_1}\right)^{\frac{1}{2}} \tag{4}$$

and the normal and tangential components of the Mach numbers are related as $M_{1n} = M_1\cos\alpha$, $M_{1t} = M_1\sin\alpha$, and $M_{2t} = M_{1t}\sqrt{T_1/T_2}$. The "sharp" interface

assumes back reflections off it and associated losses of the shock energy; thus, the ratio $M_2/M_1 < 1$. For an interface of a "smooth" type, when parameters across its thickness change slower than $1/x^2$, there are no losses associated with the shock reflection. Thus, M_2/M_1 approaches the unit, and the refraction effects become stronger [33]. An intermediate boundary type, when the parameters across its thickness can change faster than $1/x^2$ (an "extended" interface), has been considered in [34]. For a particular case of the exponential gradient in the parameter change, Eq. (3) can be replaced with more general $V_{2x}/V_1 = (T_2(x)/T_1)^{\beta}$, where $\beta = 1/2 - 1/\Sigma$ and $\Sigma = \left(\sum_{n=0}^{10} n\alpha_n + \sum_m m\alpha_m\right) = 53.58$ is the numerical constant calculated from the fit coefficients α_n and α_m in the equation:

$$\frac{T_2}{T_1} = \sum_{n=0}^{10} \alpha_n \left(\frac{M_1}{M_2}\right)^n + \sum_m \alpha_m \left(\frac{M_1}{M_2}\right)^m \tag{5}$$

The numerical constants are valid within the limits for M_1 = (1.6–2.4), T_2/T_1 = (0–75), and k = 1.4 (air). The power coefficients m in the second sum run the values m = 1/16, 1/8, ¼, and ½. In Eq. (5), the coefficient β approaches exactly ½ for a limiting case of a smooth boundary and a value much smaller than ½ for another limit of a sharp boundary [34].

3. Basic modifications in the flow: numerical simulation results and comparison with experiment

To demonstrate how the shock refraction on the interface with plasma triggers the chain of consecutive transformations in the flow, the model was numerically run for three types of plasma density distribution that would cover the most common ways of the plasma production. A relatively uniform distribution law is commonly observed in microwave discharges [37] or when the plasma spot was initiated at a considerable distance from the body shock. The exponential density distribution can be established during the exothermal expansion, for example, in large-area plasma sources created with internal low-inductance antenna units [38], detonation, or the ultra-intense laser-induced breakdown in a gas [39]. And the power law density distribution can be found in the heated layers/spheres in thermodynamic equilibrium (for both media and radiation) in the presence of radiative heat conduction, as, for example, on stellar surfaces where it is formed as the result of the combined action of gravity, thermal pressure, and radiant heat conduction [24]. On the laboratory scale, the examples of such systems include: the gas of radiative spherical cloud when simultaneously considering the mechanical equilibrium and radiative transfer, in the diffusion approximation; a planar problem of the sudden expansion into vacuum of a gas layer with a finite mass and constant initial gas distribution; a problem of sudden expansion of a spherical gas cloud into vacuum; isentropic flows for which there is a class of self-similar solutions, such as for a strong explosion on a solid surface due to other body impact with generation of vapor cloud expanding into vacuum [40]; vaporization of the anode needle of a pulsed x-ray tube caused by a strong electron discharge [41]; explosion of wires by electric currents in vacuum systems; spark discharge in air in the early stages; the gas area near the edge of a cooling wave; motion of gas under the action of an impulsive load; the spherical shock wave implosion; a problem of bubbles collapsing in a liquid [40]; in the gas behind a weak blast wave [42].

The main difference in the treatment imposed by the nonhomogeneous plasma parameter distributions is that the refracted shock velocity becomes time dependent and the system of Eqs. (1)–(3) must be substantially modified. While the plasma parameter distribution will vary, the cold gas parameters will be always considered as distributed homogeneously. For easier comparison, all the simulation results presented below will be obtained for the same incident shock strength, heating intensity, and the interface parameters, with $M_1 = 1.9, T_1 = 293$ K, $T_1/T_2 = 0.10$, equal radii $R_s = R_b$, adiabatic index $k = 1.4$ (air), and smooth boundary type. The timely order in the sequence of the flow modification stages demonstrated below follows from the model logic and agrees well with that observed in experiments: the shock front distortion and its weakening; flow parameter redistribution and pressure drop in the post-shock flow, followed with the body drag reduction; vortex generation in the plasma volume; and finally deformation or collapse of the plasma bubble.

3.1 Shock front distortion

When the temperature/density in plasma is distributed uniformly, the relations Eqs. (1)–(3) apply. Results of numerical simulation in **Figure 2** obtained for this case demonstrate the shock front distortion as it progresses through the hot plasma sphere, at different propagation times starting at $n = 0.05$ (the most left curve) through $\Delta n = 0.05$ time intervals. To highlight the size of the interface effect, the results are plotted comparatively, with the upper part of the diagram corresponding to the smooth, lower, and sharp type of the interface.

The initially spherical front acquires a nearly conical shape stretched in the propagation direction, in good agreement with the experimental observations. The most central part of the front (near the longitudinal symmetry axis) is affected by significant stretching due to longer interaction times and smaller angle of incidence. The curvature sign changes from negative to positive, with the inflection point location tending the intermediate area off the axis. Comparison between upper and lower curves shows that both types of the boundary produce identically shaped fronts; however, the smooth boundary results in stronger effect.

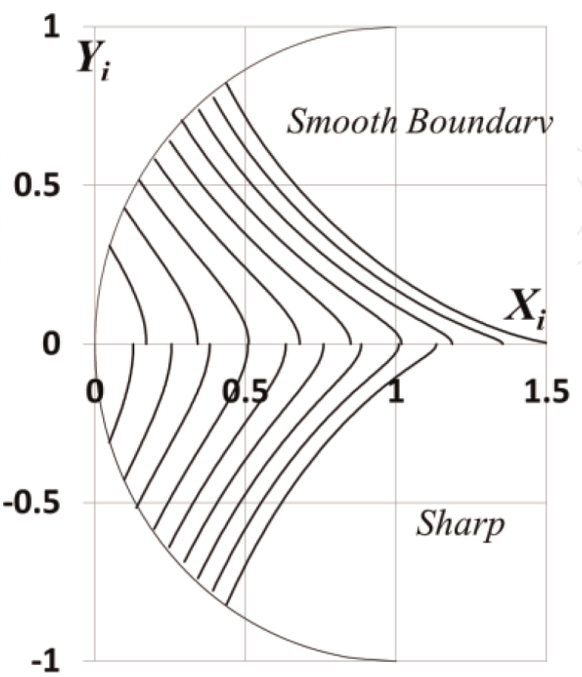


Figure 2.
The shock front modification in homogeneous plasma, at several interaction times. The shock is incident from left to right. The outside part of the shock remains spherical (not shown in the picture).

In the case of exponential plasma density distribution, the refracted shock velocity becomes dependent on time. Such a problem was considered in [19] assuming that the plasma density is exponentially decreasing in the shock propagation direction only, $\rho = \rho_{00}\, Exp\ (-x/z_0)$, starting from some finite value ρ_{00} at the leftmost point of the interface (z_0 is the characteristic length). The approximation neglecting the density change in the transverse direction can be applied, for example, to the case of plasma created by a laser sheet, with its body extended in the longitudinal direction. The task is reduced to obtain two separate solutions to the problem that must be tailored at the interface. The first solution models the shock wave refraction on the interface giving its speed and direction, and the second one describes its propagation in the inhomogeneous medium after crossing the interface. Using the approach [19] modified here for the sphere-to-sphere problem geometry, the time-dependent system of equations for the front's surface coordinates can be derived.

$$X_i = \sigma(t - t_{0i} + t_\lambda)^{2/5} + \varepsilon(t - t_{0i} + t_\lambda)^{4/5} - x_0,\ Y_i = y_i - \sigma\left(t - t_{0i} + t_\gamma\right)^{2/5} - \sigma t_\gamma^{2/5} \tag{6}$$

where $x_0 = \sigma t_\lambda^{2/5} + \varepsilon t_\lambda^{4/5}$, $t_{0i} = \frac{(x_i + x_b)}{V_1}$, $t_\gamma = \left(5V_1 \cos\alpha_i \sin\gamma_i \sqrt{\frac{T_2}{T_1}}\right) /$ $\{2\sigma \cos(\alpha_i - \gamma_i)\}$ and the parameter t_λ is the solution of the following equation

$$\frac{5}{2}\frac{V_1 \cos\alpha_i \cos\beta_i}{\sigma \cos(\alpha_i - \gamma_i)}\sqrt{\frac{T_2}{T_1}} = t_\lambda^{-3/5} + \frac{2\varepsilon}{\sigma} t_\lambda^{-1/5} \tag{7}$$

The parameters σ and ε in Eqs. (6) and (7) are related to the effective explosion energy E in the thermal spot and the scale of the density gradient z_0 as $\sigma = \varsigma\ (E/\rho_{00})^{1/5}$ and $\varepsilon = (K/z_0)\sigma^2$, and the numerical parameters $\varsigma = 1.075$ and $K = 0.185$ are borrowed from Ref. [43].

The simulation results presented in **Figure 3a** were obtained for the interaction times starting at $n = 0.05$ through $\Delta n = 0.05$ time intervals, $z_0 = 0.225$ cm, $\rho_1/\rho_{00} = 10$, $R_b = 0.1$ cm, and the parameters $\alpha = 7$ and $\beta = 402.79$ correspond to the specific explosion energy $E/\rho_{00} = 11.707 \cdot 10^3$J. The most striking result in this case is that such a density profile can generate virtually perfect conical shock fronts, exactly as observed in the experiment [13].

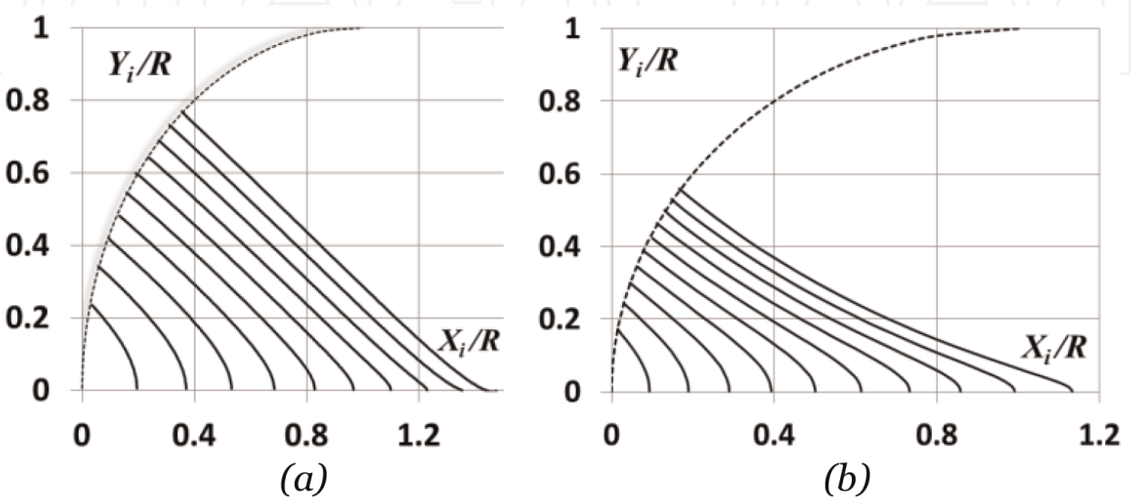


Figure 3.
Shock front deformation at several interaction times, for the cases of exponential (a) and power law (b) density distributions. Note twice as short interaction times in graph (b) compared to graph (a).

When a plane shock wave propagates through a gas with the density that drops to zero according to a power law $\rho \sim x^N$, the so-called energy cumulation effect takes place [44]. In the gas-dynamical approximation, a strong plane shock wave propagating in such a medium accelerates very quickly accumulating virtually infinite energy. This interesting phenomenon, as applied to the shock refraction problem, was considered in [35] assuming the plasma density as changing in the longitudinal (x-) direction only. Applying it to the present geometry, the refracted shock coordinates can be determined as

$$X_{2i} = a_i - (G_i/b)(t_{0i} - t)^b,\ Y_{2i} = y_i - (V_2/V_1)\sin\gamma[nR - (x_i + x_b)] \tag{8}$$

the shock velocity component $V_{2xi} = G_i(t_{0i} - t)^{b-1}$, $a_i = a - R_b(1 - \cos\alpha_i)$,

$$G_i = \frac{V_1 \cos\gamma_i \sqrt{\cos^2\alpha_i \cdot (T_2/T_1)(M_{2n}/M_{1n})^2 + \sin^2\alpha}}{[t_{0i} - ((x_i + x_b)/V_1)]^{b-1}} \tag{9}$$

$$t_{0i} = \frac{b(a - R_b(1 - \cos\alpha_i))}{V_1 \cos\gamma_i \sqrt{\cos^2\alpha_i \cdot (T_2/T_1)(M_{2n}/M_{1n})^2 + \sin^2\alpha}} + \frac{(x_i + x_b)}{V_1} \tag{10}$$

and the shock velocity ratio V_2/V_1 is determined from Eq. (3). Here a and a_i are the maximum (from the point O in **Figure 1**) and the local (from the boundary, at the periphery from the axis) distances to the zero density plane correspondingly, t_{0i} is the local time of the shock front portion travel to the boundary, the constant b = 0.59 was determined in [44], and the constant N = 3.25 is taken from [40].

The system of Eqs. (8)–(10) was run for the distance to the zero density plane a = 3.0R_b, at times starting at n = 0.025 through the equal increments Δn = 0.025 (note that the interaction times here are twice as short than in **Figure 3a**). The results presented in **Figure 3b** demonstrate considerably stronger stretching of the shock front per unit of time due to significant front acceleration in the plasma area.

Thus, as seen from **Figures 2** and **3**, the most common type of the front deformation for all three types of the density distribution is its continuous stretching. To make more exact conclusion about the front distortion, the local front inclination angle was computed, for M_1 = 1.9, T_2/T_1 = 10.0, and the smooth type of the interface.

In **Figure 4a**, the angles are presented for the uniform law of distribution, at times starting at n = 0.05 through the intervals Δn = 0.05, and the radii of the incident shock front and the interface are $R_s = R_b$ = 0.3 cm. The curves in **Figure 4b** are for the angles corresponding to the exponential law of distribution, at the same

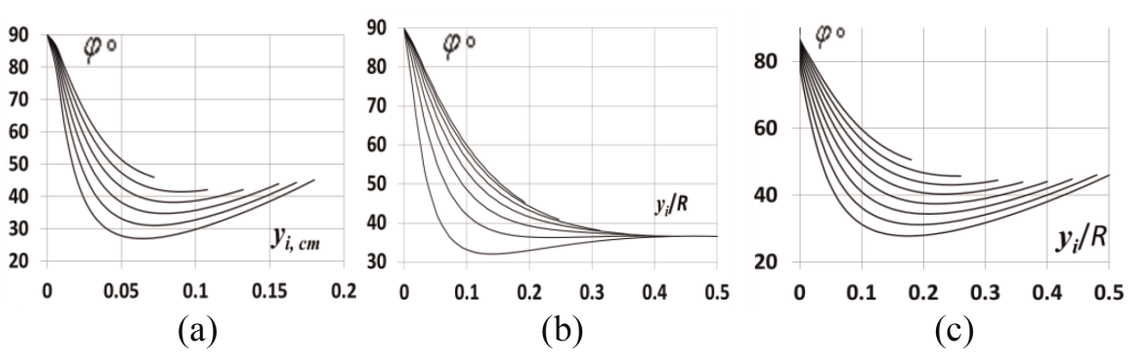


Figure 4.
The shock front inclination angle φ vs. distance y_i, at several interaction times, for the uniform (a), exponential (b), and power law (c) density distributions. The time sequence for the curves is from upper to lower.

times as in **Figure 4a**, for z_0 = 0.225 cm and σ = 7, and that in **Figure 4c** are for the power law of the distribution at shorter times, n = 0.025 through the intervals Δn = 0.025. The time sequence for the curves in all graphs is from upper to lower. The minimum angle corresponding to a location next to the longitudinal symmetry axis is common for all three types of the distribution. The angle increase to 90° as $y_i > 0$ is due to normal incidence at this point.

3.2 Pressure drop and drag reduction

In experiments, at the time when the gas pressure around the body significantly drops, recordings also show that the image of the front part of the shock wave becomes blurred or invisible and the deflection signals appear weaker and widened with time (shock "dispersion" and "disappearance") [10, 12]. As was seen above, continuous stretching of the shock front during its advancement through the plasma transforms it from being nearly normal into an inclined one. Due to the inclination, its progressively weakened intensity results in vanishing compression across the shock. As a result, the gas pressure in the flow in front of the body is lowered. If this continues, the shock wave degenerates in an ordinary pressure wave that becomes unidentifiable in the experiments.

The effect of the shock deformation on the pressure drop can be estimated through the change in the Mach number. For the homogeneous density distribution in plasma, the local inclination angle of the front φ, as defined through the tangent line, can be used to estimate the local parameter jump across the front. For this, the expressions for gas parameter variation across the normal shock front can be corrected, with the total Mach number replaced with its normal to the front component $M_{2n} = M_2 \sin(\varphi\text{-}\gamma)$. Then the pressure jump across the refracted shock $p_{21}^{(\mathrm{ref})}$ normalized to the one across the incident shock $p_{21}^{(\mathrm{inc})}$:

$$p_{21} = \frac{p_{21}^{(ref)}}{p_{21}^{(inc)}} = \frac{(2k/(k+1))M_{2n}^2 - (k-1)/(k+1)}{(2k/(k+1))M_1^2 - (k-1)/(k+1)} \tag{11}$$

In defining this parameter, the incident shock was taken as normal. This approximation works best for the area of the most strong interaction (near the symmetry axis area) or when the thermal spot dimensions (R_b) are considerably smaller compared to the incident shock radius R_s.

In **Figure 5a**, the simulation results for pressure p_{21} in the uniform density distribution case is presented, at times starting at n = 0.05 through Δn = 0.05 increments. Matching with the data in **Figures 2a** and **4a**, it is seen that the pressure

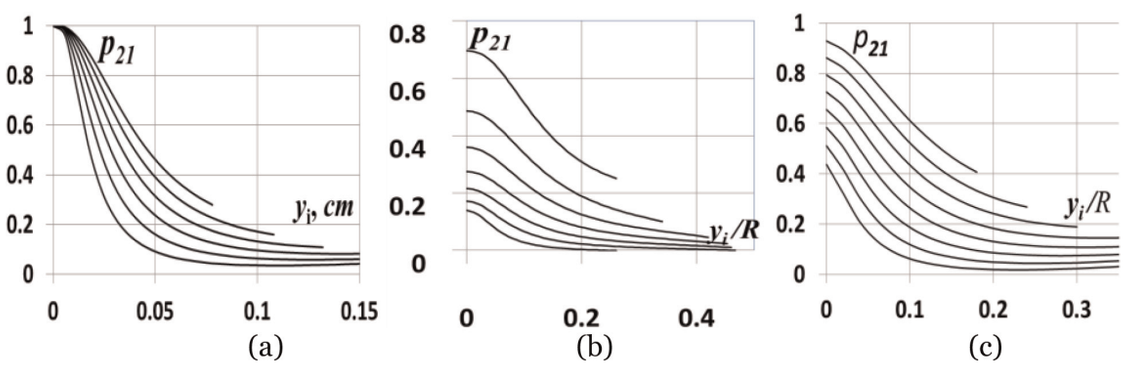


Figure 5.
Pressure ratio p_{21} vs. coordinate y_i, for the following plasma density distribution laws: (a) uniform, (b) exponential, and (c) power law. The time sequence for the curves is from upper to lower.

distribution quite closely follows the inclination angle change suggesting that this angle is the key parameter in the phenomenon.

On the axis (y_i = 0), the pressure ratio stays the same as for the incident shock due to normal position of the front relative to the propagation direction (φ = 90°).

For the exponentially distributed density, the Mach number

$$M_{2x}(t) = \left[\sigma(t - t_{0i} + t_\lambda)^{-3/5} + \varepsilon(t - t_{0i} + t_\lambda)^{-1/5}\right] / \left(20.043\sqrt{10T_1 \exp\{X_{2i}(t)/z_0\}}\right) \tag{12}$$

becomes time dependent, and the front deformation develops with an acceleration. The results for p_{21}, obtained for times starting at n = 0.05 through Δn = 0.05 increments, z_0 = 0.225 cm, σ = 7, and R_s = 0.1 cm, are presented in **Figure 5b**. For the most part of the shock front, the pressure significantly drops, with the distribution closely matching the inclination angle change (**Figure 4b**). The pressure ratio levels are in good agreement with the observations of cone-shaped fronts [13] where the reduction by three to four times in the pressure in the central area of the shock front and almost zero pressure at the stagnation point is typical.

Compared to the two previous cases, the effect of the power law density distribution is stronger (**Figure 5c**): the front becomes deformed to a larger degree and moves considerably faster (note twice as short interaction times, starting at n = 0.025, with Δn = 0.025 increments). The pressure ratio drops to the levels between 0.25 and 0, and the compression in the shock becomes weaker as it approaches the 0 density point. This is possible despite the sharp increase in the velocity because the density ahead of the wave decreases faster, similarly to the case of a plane shock propagating through an unbounded plasma medium [40].

Since the gas pressure in front of the moving body becomes significantly lowered, the decrease in the drag follows. In the spherically symmetrical case, the drag can be numerically estimated by summing the longitudinal pressure component over the body's surface $d = \sum_i 2\pi r_i p_i \cos\alpha_i - d_b$, where α_i is the local angle of incidence on the body and d_b is the summing result for the back body surface. While the total drag experienced by the body is dependent on its shape, it is still linearly proportional to the ambient pressure and will decrease accordingly. The drag reduction about 2–2.5 times recorded in experiments, at the times when the shock modification occurred, confirms these conclusions.

3.3 The parameter redistribution in the flow and generation of vorticity

As a result of refraction, the initially horizontal shock velocity vector rotates at local refraction angle γ_i, and thus the velocity acquires an additional, location-dependent y-component. Then the velocity components for the flow behind the shock

$$v_x = v_n \sin\varphi + V_2 \cos(\varphi - \gamma)\cos\varphi, v_y = v_n \cos\varphi - V_2 \cos(\varphi - \gamma)\sin\varphi \tag{13}$$

result in non-zero vorticity [45] that can be calculated at specific locations along the shock front surface as

$$\omega_i = \omega_i(X_i, Y_i) = \left(\partial v_x/\partial y - \partial v_y/\partial x\right)_{x=X_i,\, y=Y_i} \tag{14}$$

Thus, in addition to the rotation of the shock velocity vector at an angle γ, there is a turn for the flow velocity relative to its initial propagation direction, at the angle

$g = tan^{-1}(v_y/v_x)$. The shock wave and the flow behind it will diverge at a relative angle $\xi = tan^{-1}(v_y/v_x) - \gamma$ (double refraction) giving rise to a non-zero circulation in the hot gas volume.

Numerical results for dimensionless vorticity $\overline{\omega} = \omega_i/(V_1/R_b)$ developing in the flow with the homogeneous plasma parameter distribution vs. the coordinate Y_i are presented in **Figure 6a**, for times between $n = 0.18$ and 0.42 with $\Delta n = 0.03$ increments, and the last curve corresponds to $n = 0.44$ chosen for better resolution on the graph. The time sequence for the curves is in the up-direction. Only the upper half of the picture is shown; thus, the results on the graph correspond to a vortex sheet with rotations in both halves of the picture in opposite directions (in cylindrical geometry) or a toroidal vortex ring if considered in the spherical geometry.

Due to a small size of the structure, the Y-coordinate was scaled with the factor of 10^2, and thus the picture is greatly zoomed in on the narrow region next to the symmetry axis. The spike in the vorticity intensity observed in close proximity to the symmetry axis exactly corresponds to the location where abrupt change in the shock front structure occurs (**Figures 2a** and **4a**). This trend is pointing at the fact that the local rate of change of the front inclination angle φ is the key factor in the origin of the vorticity. The nonlinear growth of the vortex intensity (**Figure 6**) demonstrates the possibility of a strong positive dynamics in its development.

The specific effect of the exponential density distribution has been studied for the interaction times between $n = 0.05$ and 0.40 through $\Delta n = 0.05$ increments, and the last two curves correspond to $n = 0.43$ and 0.45. (**Figure 6b**). Due to practically no areas on the shock front where its shape would change sharply enough (**Figures 2b** and **4b**), except a very narrow region near the symmetry axis, significant vorticity develops mostly in this region corresponding to the very tips of the fronts. The maximum vorticity intensity is about two orders of magnitude less compared to the levels found in the uniform density distribution case. Considerably weaker vorticity and a very small size of the structure found here can probably explain why sometimes the vortex system "does not develop" in experiments even though noticeable changes in the shock structure and pressure/drag reduction are present.

In the presence of the energy accumulation effect (power law density distribution), with more stretched fronts and softer distribution of the front inclination angle φ, the vorticity develops slower (**Figure 6c**), but still, its intensity steadily grows with time at all locations on the front. The curves on the graph correspond to times $n = 0.025$–0.250 with 0.025 increments and the distance $a = 3.0R_b$. The vorticity originates further from the symmetry axis confirming a larger size of the vortex structure. As in other density distribution cases, the maxima of vorticity (centers) shift toward each other as the shock advances through the volume, following the same trend for the sharpest bending on the front and the shock and flow rotation angles to move closer to the axis [45]. The total vorticity intensity

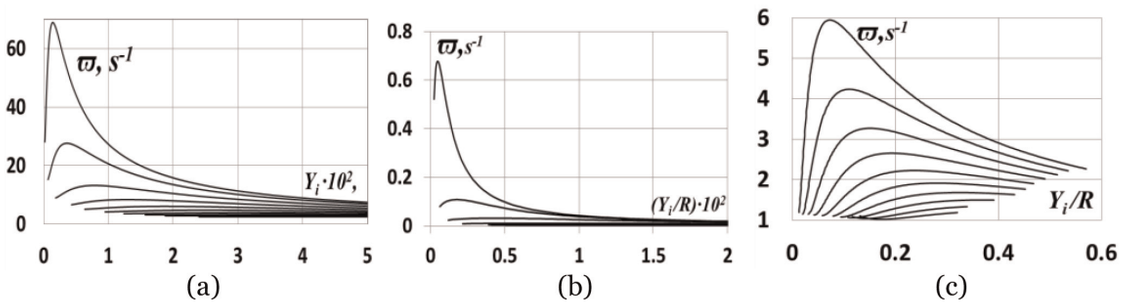


Figure 6.
Dimensionless vorticity ϖ vs. Y_i, for the uniform (a), exponential (b), and power law (c) density distributions. The time sequence is from lower curve to upper.

integrated over the whole plasma volume becomes considerably higher compared to the uniform density case because of the contribution from the regions located further from the axis. The same strong correlation between shock deformation, vortices of similar size, rotational direction, and topology with pressure/wave drag drop evolving in the same sequence and within the same time frames was confirmed in [46].

3.4 The interface stability problem

The existence of phenomenological connection between the shock's and the interface stability makes the chain of the transformations in the flow to continue. Since the flow instabilities take place upstream from the interface, the perturbations to the flow parameters propagating downstream, toward the interface, will disturb it. The overall pressure drop behind the refracted shock continuously mounting with time is responsible for the sucking effect resulting in the large-scale interface perturbation, moving it closer to the shock. The positive and essentially nonlinear dynamic in the pressure perturbation evolution [17] will support amplification of this global perturbation to the interface and thus determines the pattern in the interface instability structure. With increasing distortion of the interface, Kelvin-Helmholtz (KH) shearing instability may start to contribute resulting in the characteristic mushroom shapes of the interface perturbations [47]. The initial instability pattern associated with the global pressure drop behind the refracted shock will be of a larger scale, and the KH instability turning on at later stages would finally determine the smaller characteristic structure.

4. Conclusion and controlling the drag

The sequence of interconnected stages of the flow modification described here, in fact, is a complex way of the shock flow instability development that is triggered via the single mechanism of the shock refraction on an initially disturbed (curved) interface. At the moment of exiting the interface disturbance, the shock wave reaches a new stable state characterized by a new front structure and the gas parameter distribution behind it. The instability starts to develop in the form of a wavelike shock front stretching into the lower density plasma, and the global pressure drop is the consequence of the weakened shock wave. Pressure perturbations caused by the shock stretching result in the loss of stability of the flow behind it that eventually organizes into an intense clockwise rotating vortex structure. If the plasma density is nonuniform, the transition in the form of front stretching exhibits the pattern of motion that prevails the principle of exchange of stabilities, so the instability sets in as a secondary flow. Regardless of the interaction geometry, the instability mode is aperiodical and unconditional, and thus either a transition to another stable state or continuous development as a secondary flow is possible. The marginal state condition $\{T_2/T_1 > (M_1/M_2)^2, |\chi| > 0\}$ is the only requirement to trigger the instability [17], where the minimum heating requirement accounts for losses due to shock reflections off the interface. Independence of the instability locus on the plasma density distribution identifies the interface conditions as the sole triggering factor, though the density gradient can discriminate between qualitatively different outcomes at later stages of the instability evolution. With T_{21} fixed, in the uniform density case, the perturbation growth rates are determined solely by the interface perturbation curvature χ that, for some geometries, can be replaced with the *relative* curvature between the shock front and the interface. The specific wave nature of the instability dissipation, when the overstretched shock

perturbation decays via the degeneration into an acoustic wave, allows the shock instability to decay even though the viscous damping mechanisms are not available in the flow (except the shock width layer). The initial state shock wave energy, in this case, converts into rotational energy of the flow thus continuously supporting the developing vortex structure until the perturbed shock vanishes.

The advantage of the model presented here is that it provides useful insight on the phenomenological origin of the drag reduction and its connection to the series of other phenomena that accompany the interaction. Its simple analytical solutions can be used for quick estimates and thus avoid the complexity of more exact numerical calculations. The dimensionless form of the equations and similarity law found in the spatial and temporal evolution of the flow perturbations with respect to the interface curvature [17] allow conclusions to be applied to any scale of the interaction. Though the model here was specifically developed for the spherical or sphere-to-flat (as a limiting case) geometry of the interaction, the equations can be readily modified for other configurations. The shock reflections off the interface can be accounted in the model to its various degrees with the Mach number ratio M_{2n}/M_{1n} different from the unit [34], thus accommodating various types of the interface. Note that even plasma as a medium inside the heated area was considered, the nature of the effect is purely thermal and hence the model can be applied to conditions where only thermal heating in a neutral gas is present.

It was shown here that gas parameter redistribution in the flow behind the refracted shock front, including the global pressure drop, is the cause for the vorticity generation rather than its consequence. Thus, the pressure drop and the vortical perturbations in the post-shock flow can be considered rather competing because of the locally developing secondary flows resulting in an effective mixing. This eventually equalizes pressure in different parts of the volume and thus quenches (at least partially) the pressure drop and large-scale sucking effect on the interface. Thus, if pressure lowering is thought, the vortex generation must be minimized. Then the parameters of the interaction must be chosen in such a way that the shock front would be stretched considerably and as possible evenly, without sharp bends causing intensive vorticity. Spherical geometry and the exponential type of the plasma parameter distribution would be the best fit for this purpose as it was shown to generate vorticity of either micro-size and/or micro-intensity. Thus, the choice of the plasma parameter distribution alone can offer the advantage of depositing less energy of a smaller volume and closer to the body.

Other applications where the vorticity development must be avoided include magnetized target fusion experiments, for example, where, during the implosion of an inertial confinement fusion target, the hot shell materials surrounding the cold D-T fuel layer are shock-accelerated [25]. Mixing of the shell material and fuel is not desired in this case, and efforts should be made to minimize any abrupt imperfections or irregularities on the shock front. Considering a sharp type of the interface can be helpful in such cases since the refraction effect can be up to 40% weaker [18].

Contrary, in the applications where vorticity is beneficial for better mixing in the flow, sharp distortions spanning a larger portion of the shock front are necessary, and the uniform and the power law density distributions could be more desirable in this case. The examples include combustion where the burning speed is controlled by introducing turbulence in the flow [22]. A supersonic combustion in a scramjet may also benefit from vorticity in the flow as the fuel-oxidant interface is enhanced by the breakup of the fuel into finer droplets. Studies of deflagration to detonation transition (DDT) processes show that introduction of vorticity can result in an increase in burning velocity and detonation. In this case, introducing small perturbations of the interface that will cause sharp distortions on the shock front can be suggested [17].

In optimizing the ratio R_s/R_b, it should be noted that the interaction can be less significant if the size of the thermal spot becomes small compared to the shock front dimensions. It is not only because of a relatively smaller plasma volume or deposited energy but also due to smaller relative curvature of the shock front as seen from the plasma boundary (approaching a nearly flat shape as $R_s/R_b \to 0$). This results in shorter interaction time and consequently weaker effect. Higher temperature/density step across the interface and the smooth interface type can be also used to strengthen the effect.

In discussing validity of the model for a particular application, the following factors must be taken into consideration. First, the model assumes that the plasma region is not expanding, i.e., that the gas is in an equilibrium state. With the interaction times on the order of 0.1 μs and in the temperature range typical for many thermal energy deposition experiments, the approximation works well, for example, for diatomic gases whose vibrational relaxation times are on the order of tens of microseconds or longer (at atmospheric pressure). However, for considerably elevated gas temperatures or pressures and in specific gases, the relaxation times may become comparable to the interaction time, and the model would need a correction for non-equilibrium effects.

Second, the model does not assume various degree deformation of the plasma region during the interaction time and thus should be considered as a valid approximation only when the coupling between the shock flow and the interface instability can be neglected. The model also assumes the ideal gas conditions. For the pressures typically developed in the shocks, the gas state equation can be still valid. However, the parameter jump relations across the shock in real gases may depart from their ideal equivalents significantly, and Eq. (4) must be corrected. An analysis of such effects must be done, and the criteria of ideality have to be applied and tested in the experiments used for comparison. For most energy deposition conditions though, the approach developed here appears to be quite adequate as, within the time frame of the interaction, the model predictions in the form of consistent time and dimension relationship are clearly visible in most of the experiments [12, 22].

The shock refraction on an interface was considered here as the main mechanism of the wave drag reduction. The contribution of other thermal or nonthermal secondary mechanisms should be accounted for as well. In addition to those mentioned in the introduction, these can include the mechanisms participating in the formation of the thermal equilibrium and definite parameter distribution in the plasma during rapid expansion of the thermal spot. A blast wave produced at the early stages of the plasma creation can result in the pressure increase on the body at the first moment followed by the main pressure and the drag drop [48]. This may interfere with the shock refraction effects and overlap with the processes described in the model. The mechanisms controlling the effectiveness of the energy transfer to the gas during its deposition to the flow should be taken into account for better optimization.

The results of this work can be found useful in a number of other major applications. With optimized energy deposition, decreased pressure with an extended rise time on the ground can be used to alleviate the sonic boom or reduce the heating of a space craft at atmospheric entry. Other potential areas of application include magnetohydrodynamics (MHD), plasma chemical reactors, and molecular lasers for shock wave structure control; rocket plume optimization; shock wave-assisted combustion, where a shock wave can be used to affect the ignition conditions in the gas; plasma-based piloting and combustion enhancement that can be used toward the design of efficient combustors for hypersonic propulsion systems, combustors for gas turbine, diesel engines, environmentally clean combustors, and spark inhibition; localized flow problems, such as the Edney type IV shock

interaction and the control of shock structures formed in the high-speed engine inlet; and astrophysics for understanding the dynamics of shock waves generated in the stellar interior.

IntechOpen

IntechOpen

Author details

Anna Markhotok
Physics Department, Old Dominion University, Norfolk, VA, USA

*Address all correspondence to: amarhotk@phys.washington.edu

IntechOpen

© 2019 The Author(s). Licensee IntechOpen. This chapter is distributed under the terms of the Creative Commons Attribution License (http://creativecommons.org/licenses/by/3.0), which permits unrestricted use, distribution, and reproduction in any medium, provided the original work is properly cited. CC BY

References

[1] Bushnell D. Shock wave drag reduction. Annual Review of Fluid Mechanics. 2004;**36**:81-96. DOI: 10.1146/annurev.fluid.36.050802.122110

[2] Carlson HW, Mack RJ. Studies of leading edge thrust phenomena. In: 18th AIAA Aerospace Sciences Meeting; Pasadena, CA: AIAA Paper; 1980. pp. 80-0325.

[3] Jones RT. Aerodynamic design for supersonic speeds. In: Karman V et al., editors. Advances in Aeronautical Sciences. New York: Pergamon; 1959. pp. 34-51

[4] Jones RT. The flying wing supersonic transport. Aeronautical Journal. March 1991;**95**(943):103-106

[5] Bushnell DM. Supersonic aircraft drag reduction. In: AIAA 21st Fluid Dynamics and Plasmadynamics Lasers Conference; Seattle, WA: AIAA Paper; 1990. pp. 90-156

[6] Kuflan RM. Application of favorable aerodynamic interference to supersonic airplane design. SAE Technical Paper; 901988; Warrendale, PA: SAE; October 1990

[7] Bur R, Corbel B, Delery J. Study of passive control in a transonic shock wave/boundary layer interaction. AIAA Journal. 1997;**36**(3):394-400

[8] Reneaux J, Coustols E, Wave drag reduction technologies. In: Onera-DLR Aerospace Symposium; Paris; 1999

[9] Austin F, Siclari MJ, Van Nostrand WC, Weisensel GN, Kottamasu V, Guiseppe V. Comparison of smart wing concepts for transonic cruise drag reduction. In: Proceedings of SPIE-The International Society for Optical Engineering; 3044; Bellingham, WA; 1997. pp. 33-40

[10] Kuo SP. Shock wave modification by a plasma spike: Experiment and theory. Physica Scripta. 2005;**71**:535-539

[11] Zukovski E, Spaid F. Secondary injection of gases into a supersonic flow. AIAA Journal. 1964;**2**(10):1689-1696

[12] Erdem E, Kontis K, Yang L. Steady energy deposition at Mach 5 for drag reduction. Shock Waves. 2013;**23**(4): 285-298. DOI: 10.1007/s00193-012-0405-8

[13] Satheesh K, Jagadeesh G. Experimental investigations on the effect of energy deposition in hypersonic blunt body flow field. Shock Waves. 2008;**18**:53-70

[14] Kremeyer K, Sebastian KA, Shu C-W. Computational study of shock mitigation and drag reduction by pulsed energy lines. AIAA Journal. 2006;**44**: 1720-1731

[15] Guvernyuk S, Samoilov A. Control of supersonic flow around bodies by means of a pulsed heat source. Technical Physics Letters. 1997;**23**:333-336

[16] Schulein E, Zheltovodov A, Pimonov E, Loginov MS. Experimental and numerical investigations of electric-arc air spikes for blunt and sharp bodies at Mach 5. In: International Conference on Methods of Aerophysical Research, ICMAR; 2008

[17] Markhotok A. A shock wave instability induced on a periodically disturbed interface. IEEE Transactions on Plasma Science. 2018;**46**(8): 2821-2830. DOI: 10.1109/TPS.2018.2848597

[18] Markhotok A, Popovic S. Refractive phenomena in the shock wave dispersion with variable gradients. Journal of Applied Physics. 2010;**107**: 123302

[19] Markhotok A, Popovic S. Redirection of the spherical expanding shock wave on the interface with plasma. Physics of Plasmas. 2014;**21**: 022105

[20] Marconi F. An investigation of tailored upstream heating for sonic boom and drag reduction. AIAA Journal. 1998;**333**:1-6

[21] Sasoh A, Ohtani T, Mori K. Pressure effect in shock-wave-plasma interaction induced by a focused laser pulse. Physical Review Letters. 2006;**97**: 205004

[22] Thomas GO, Bambrey RJ, Brown CJ. Experimental observations of turbulent combustion and transition to detonation following shock-flame interaction. Combustion Theory and Modelling. 2001;**5**:573-594

[23] Georgievskii PY. Transition to Irregular regimes of supersonic flows over bodies initiated by energy deposition. In: 43rd AIAA Aerospace Sciences Meeting and Exhibit; Reno, NV; 2005

[24] Frank-Kamenetskii DA. Non-adiabatic pulsations in stars. Doklady Akademii Nauk SSSR. 1951;**80**:185 (In Russian)

[25] Suponitsky V, Barsky S, Froese A. On the collapse of a gas cavity by an imploding molted lead shell and Ritchmer-Meshkov instability. Bonneville Place, Burnaby, Canada: General Fusion Inc.; 2013

[26] Ju Y, Shimano A, Inoue O. Vorticity generation and flame distortion induced by shock flame interaction. Symposium (International) on Combustion. 1998; **27**(1):735-741

[27] Bray KNC. In: Libby PA, Williams FA, editors. Turbulent Reacting Flows, Topics in Applied Physics. Vol. 44. Berlin: Springer; 1980

[28] Shneider M. Energy addition into hypersonic flow for drag reduction and steering. In: Atmospheric Pressure Weakly Ionized Plasmas for Energy Technologies, Flow Control and Materials Processing. August 22–24, 2011; Princeton, NJ

[29] Khorunzehenko V, Roupassov D, Starikovskii A. Hypersonic flow and shock wave structure control by low temperature nonequilibrium plasma of gas discharge. In: 38th AIAA/ASME/ SAE/ASEE Joint Propulsion Conference and Exhibition; AIAA 2002-3569. 2002

[30] Kuo SP. Shock wave mitigation by air plasma deflector. Advances in aerospace science and technology. 2018; **3**:71-88

[31] Satheesh K, Jagadeesh G. Effect of concentrated energy deposition on the aerodynamic drag of a blunt body in hypersonic flow. Physics of Fluids. 2007;**19**(3):031701

[32] Batley GA, McIntosh AC, Brindley J. The baroclinic effect in combustion. Mathematical and Computer Modelling. 1996;**24**(8):165-176

[33] Markhotok A. The mechanism of wave drag reduction in the energy deposition experiments. Physics of Plasmas. 2015;**22**:063512

[34] Markhotok A, Popovic S. Shock wave refraction enhancing conditions on an extended interface. Physics of Plasmas. 2013;**20**:4

[35] Markhotok A. The cumulative energy effect for improved ignition timing. Physics of Plasmas. 2015;**22**:043506

[36] Alexandrov AF, Vidiakin NG, Lakutin VA, Skvortsov MG, Timofeev IB, Chernikov VA. Potential mechanism of shock-wave interactions with decomposing plasma of laser spark in the air. Zhurnal Tekhnicheskoi Fiziki. 1986;**56**:771

[37] Kessaratikoon P, Markhotok A, Brooke G, Popović S, Vušković L. Shock wave dispersions in microwave discharges. Bulletin of the American Physical Society. 2002;**47**:43

[38] Deguchi H, Yoneda H, Kato K, Kubota K, Hyashi T, Ogata K, et al. Size and configurations in large-area RF plasma production with internal low-inductance antenna units. Japanese Journal of Applied Physics. 2006;**45**: 8042-8045

[39] Bret A, Deutsch C. Beam-plasma electromagnetic instabilities in a smooth density gradient: Application to the fast ignition scenario. Physics of Plasmas. 2005;**12**:102702

[40] Zeldovich YB, Raizer YP. Physics of Shock Waves and High-Temperature Hydrodynamic Phenomena. New York and London: Academic Press; 1967

[41] Tsukerman V, Manakova M. Sources of short X-ray pulses for investigating fast processes. Soviet Physics Technical Physics (English Translation). 1957;**2**:353-363

[42] Bah G, Lee J. An analytical solution for blast waves. AIAA Journal. 1970;**8**: 271-275

[43] Andriankin EI, Kogan AM, Kompaneets AS, Krainov VP. Propagation of a strong explosion in an inhomogeneous atmosphere. Zhurnal Prikladnoi Mekhaniki I Tekhnicheskoi Fiziki. 1962;**6**:3-7 (In Russian)

[44] Sakurai A. On the problem of a shock wave arriving at the edge of gas, commune. Pure and Applied Mathematics. 1960;**13**:353-370

[45] Markhotok A. A mechanism of vorticity generation in a supersonic flow behind an interface. Fluid Dynamics Research. 2018;**50**(4):1-22. DOI: 10.1088/1873-7005/aac118

[46] Lashkov VA, Mashek IC, Anisimov YI, Ivanov VI, Kolesnichenko YF, Ryvkin MI, et al. Gas dynamic effect of microwave discharge on supersonic cone-shaped bodies. In: 42nd AIAA Aerospace Sciences Meeting and Exhibit; Reno, NV; AIAA 2004-0671. 2004

[47] Bruillette M. The Richtmeyer-Meshkov instability. Annual Review of Fluid Mechanics. 2002;**34**:445-468

[48] Knight D. Survey of aerodynamic drag reduction at high speed by energy deposition. Journal of Propulsion and Power. 2008;**24**(6):1153-1167